Article

Computational Medicinal Chemistry applications to cure Asian-prevalent strain of Hepatitis C Virus

Rashid Hussain [1,*]**, Zulkarnain Haider** [1]**, Hira Khalid** [1,*]**, M. Qaiser Fatmi** [2]**, Simone Carradori** [3]**, Amelia Cataldi** [3]**, and Susi Zara** [3]

1 Department of Chemistry, Forman Christian College University, Lahore-54000, Pakistan.
2 Department of Biosciences, COMSATS University Islamabad, Park Road, Chak Shahzad, Islamabad 45600, Pakistan
3 Department of Pharmacy, "G. d'Annunzio" University of Chieti-Pescara, via dei Vestini 31, 66100 Chieti, Italy

* Correspondence:, hirakhalid@fccollege.edu.pk (HK), rashid.bioinfo@gmail.com (RH)

Abstract: Hepatitis C Virus (HCV), affecting millions of people worldwide, is the leading cause of the liver disorder, cirrhosis, and hepatocellular carcinoma. HCV is genetically diverse having eight genotypes and several subtypes predominant in different regions of the globe. The HCV NS3/4A protease is a primary therapeutic target for HCV with various FDA-approved antivirals and several clinical developments. However, available protease inhibitors (PIs) have lower potency against HCV genotype 3 (GT3), prevalent in South Asia. In this study, the incumbent computational tools were utilized to understand and explore interactions of the HCV GT3 receptor with the potential inhibitors after the virtual screening of one million compounds retrieved from the ZINC database. The molecular dynamics, pharmacological studies, and experimental studies uncovered the potential PIs as ZINC000224449889, ZINC000224374291, and ZINC000224374456 and derivative of ZINC000224374456 from the ZINC library. The study revealed that these top hit compounds exhibited good binding and better pharmacokinetics properties that might be considered the most promising compound against HCV GT3 protease. Viability test, on primary healthy Human Gingival Fibroblasts (HGFs) and cancerous AGS cell line were also performed to assess their safety profile after administration. In addition, Surface Plasmon Resonance (SPR) was also performed for determination of affinity and kinetics of synthesized compounds with target proteins.

Keywords: Structure-based drug design, virtual screening, Cell Viability, Surface Plasmon Resonance

1. Introduction

Hepatitis C Virus (HCV) is a member of Flaviviridae family that was first discovered in 1989 [1]. According to the World Health Organization (WHO), HCV is responsible for more than 185 million infections worldwide, making it a significant global public health issue [2]. The virus is most commonly transmitted through contact with infected blood, such as sharing of needles among injection drug users, and unsafe medical procedures, including blood transfusions and organ transplants prior to the implementation of screening procedures. It can also be transmitted through unprotected sexual contact, perinatally from mother to child during childbirth, and in rare cases through occupational exposure to infected blood. HCV infections can lead to chronic hepatitis, cirrhosis, liver failure, and liver cancer, highlighting the importance of effective prevention and treatment strategies [3,4].

The HCV genome exhibits high genetic diversity, with eight major genotypes and 87 subtypes identified to date [5,6]. This genetic diversity is due to the high mutation rate in the HCV genome, i.e., 10−3 substitutions per site per year [7]. It contributes to the difficulty in developing effective vaccines and antiviral therapies against HCV. However, understanding the structure and function of the HCV genome provides insights into viral replication and pathogenesis, and can inform the development of new therapeutic strategies to combat HCV infections. The genome of the Hepatitis C Virus (HCV) is a single-stranded, positive-sense RNA molecule that contains approximately 9.6 kilobases in length. The RNA genome consists of an open reading frame (ORF), 5′ untranslated region (UTR), and 3′ UTR.

HCV encodes a single polyprotein that is processed into at least 10 individual proteins, including six non-structural (NS) proteins and three structural proteins. The NS proteins consist of ion channel (p7), auto-protease (NS2), protease and helicase (NS3), co-factor (NS4A), membrane-associated protein (NS4B), phosphor-protein (NS5A), and RNA-dependent RNA polymerase (NS5B). These proteins are responsible for various functions in viral replication, assembly, and immune evasion. NS3 has both protease and helicase activity and is essential for the replication of the HCV genome. NS5B is an RNA-dependent RNA polymerase, which is essential for viral replication, and is also the target of several antiviral drugs. NS5A is a multi-functional protein that plays a critical role in viral replication, assembly, and modulation of host immune responses. The three structural proteins include capsid (C) and envelope proteins (E1 and E2). The capsid protein forms the nucleocapsid core of the viral particle, while the envelope proteins are responsible for viral entry into host cells and are the main targets of neutralizing antibodies. E2 is also involved in viral attachment to host cells, while E1 is required for viral fusion with host cell membrane [8–10]. To cure HCV, it's important to identify the most suitable drug target. There are various tools available for this purpose, including the prediction of choke-points for drug-target identification. This process involves identifying metabolic reactions that either consume a unique substrate or produce a unique product, which can then be used as potential drug targets [11–13]. In general, both the non-structural and structural proteins of HCV are crucial to the viral life cycle and represent critical targets for antiviral therapies. Inhibition of NS3/4A protease and NS5B polymerase have been shown to be effective in treating HCV infection, and ongoing research is focused on developing new drugs that target other HCV proteins, including NS5A and the envelope proteins [14–16,16].

Currently available drugs for HCV treatment are not equally effective against all genotypes. Most of these drugs are designed to target genotype 1, while little attention has been given to developing drugs specific to genotype 3a. This is partly due to the lack of a crystal structure of NS3 GT3, which makes it difficult to design genotype-specific drugs. Recent studies have identified specific mutations at key residues that are responsible for the lower response of genotype 3a to existing drugs [7].

On the other hand, in silico calculations are among essential therapeutic strategies, particularly where the experimental structure of the target proteins has not been revealed yet. In addition, molecular modeling methods help us understand drug-target interactions and discover novel drug candidates.

Our recent studies have used several in silico tools [17–19]. Finally, to determine the safety profile of the best-in-class compounds, we assayed them at two fixed concentrations (10 and 50 μM) and discrete time points (48 and 72 h) on healthy primary Human Gingival Fibroblasts (HGFs) and a cancerous cell line (AGS, gastric adenocarcinoma) by means of the MTT test. The former cell type has been selected as they represent the first cell population to be in contact with the compounds after oral administration [20].

2. Materials and Methods

The general workflow of the research project is given in the flowchart (**Figure 1**). Initially, the computational studies were conducted to find potential inhibitors against the drug target HCV NS3 GT3. The computational results were then validated using experimental methods. The methods and techniques used in computational and experimental studies are given below.

2.1. Computational Studies

2.1.1. Homology Modelling

The homology modeling approach was used to predict the 3D model of the protease domain of NS3 protease genotype 3a using the crystal structure of HCV NS3 protease genotype 1b as a template (PDB ID: 4I31), having 100% sequence coverage and 78% sequence identity. The primary sequence of HCV NS3 genotype 3a was retrieved from NCBI (GenBank accession: AEV46286). SWISS-MODEL, an automated protein structure homology modeling server, was used to model the protein.

The target and the template sequence were aligned using the ClustalW alignment tool [21]. Finally, the modelled structure of NS3 GT3a was further evaluated for compatibility of various structural parameters using comparative assessment tools like Ramachandran Plot [22].

2.1.2. Compounds database

The clinically validated compounds reported against HCV NS3 protease include Paritaprevir, Glecaprevir, Grazoprevir, Telaprevir, Voxilaprevir Simeprevir, and Boceprevir, which were taken from Drugbank (https://go.drugbank.com/) and used as a control for the in-house compounds. The ZINC database (ZINC is not Commercial) was used for retrieving one million compounds from ZINC15 (https://zinc15.docking.org/) [23].

2.1.3. Virtual screening

The virtual screening of the retrieved compounds was performed by UCSF DOCK 6 [24] in the following steps:

(1) Receptor and Ligand Structure Preparation: The model protein of HCV NS3 GT3 was opened using UCSF Chimera. The Dock prep module of Chimera was used for receptor preparation;

(2) Sphere Generation and Selection: The binding groove sphere of 3Å was generated by using the knowledge of docked ligand of the template protein PDB ID: 4I31;

(3) Grid Generation: The grid around the receptor's active site was generated by keeping the distance between grid points along each axis;

(4) Docking: Rigid Ligand Docking was performed in which the ligand was kept completely rigid during the orientation step.

2.1.4. Molecular Dynamics Simulations

The refinement of the modelled NS3 GT3 was obtained through MD simulations using GROMACS 5.1.1 [25]. The modelled protein was checked for missing residues/atoms and then initialized by generating topologies using the OPLS-AA/L all-atom force field [26,27]. The system was solvated in an explicit water cubic box using a 3-site Simple Point Charge (SPC) model. Periodic boundary conditions (PBC) were implemented to circumvent boundary effects caused by the finite size of the system. The minimum distance between the protein system and box edge was set to at least 1.0 nm to avoid any artifact incurred by the minimum image convention. The whole system was neutralized by adding 6 Cl$^-$ ions to the environment. The plan was then energy minimized using 50,000 steps of the steepest descent minimization algorithm to avoid any bad contacts generated while solvating the system. To stabilize the environment equilibration of the system was

conducted in two phases. The first phase was conducted under an NVT ensemble (constant Number of particles, Volume, and Temperature) by keeping temperature at 300K and pressure coupling off. In second phase NPT ensemble (constant Number of particles, Pressure, and Temperature) was used to keep pressure coupling at 1 bar.

The Leap-frog integrator was used to integrate the Newtonian equation of motion with 25,000,000 steps. SHAKE algorithm was used to fix all bond distances involving hydrogen atoms; therefore, the time step was increased to 2 femtoseconds (fs), making the total duration of simulation 50 ns. The Lenard-Jones equation was used to calculate van der Waal's interactions. The short-range neighbour list cut-off, short-range electrostatic cut-off, and short-range van der Waal's cut-off were fixed at 1 nm. The conformations of the homology model generated during the 50 ns MD simulation were compared with those obtained for simulations of the template crystal structure, 4I31.pdb, performed using the same parameters and conditions.
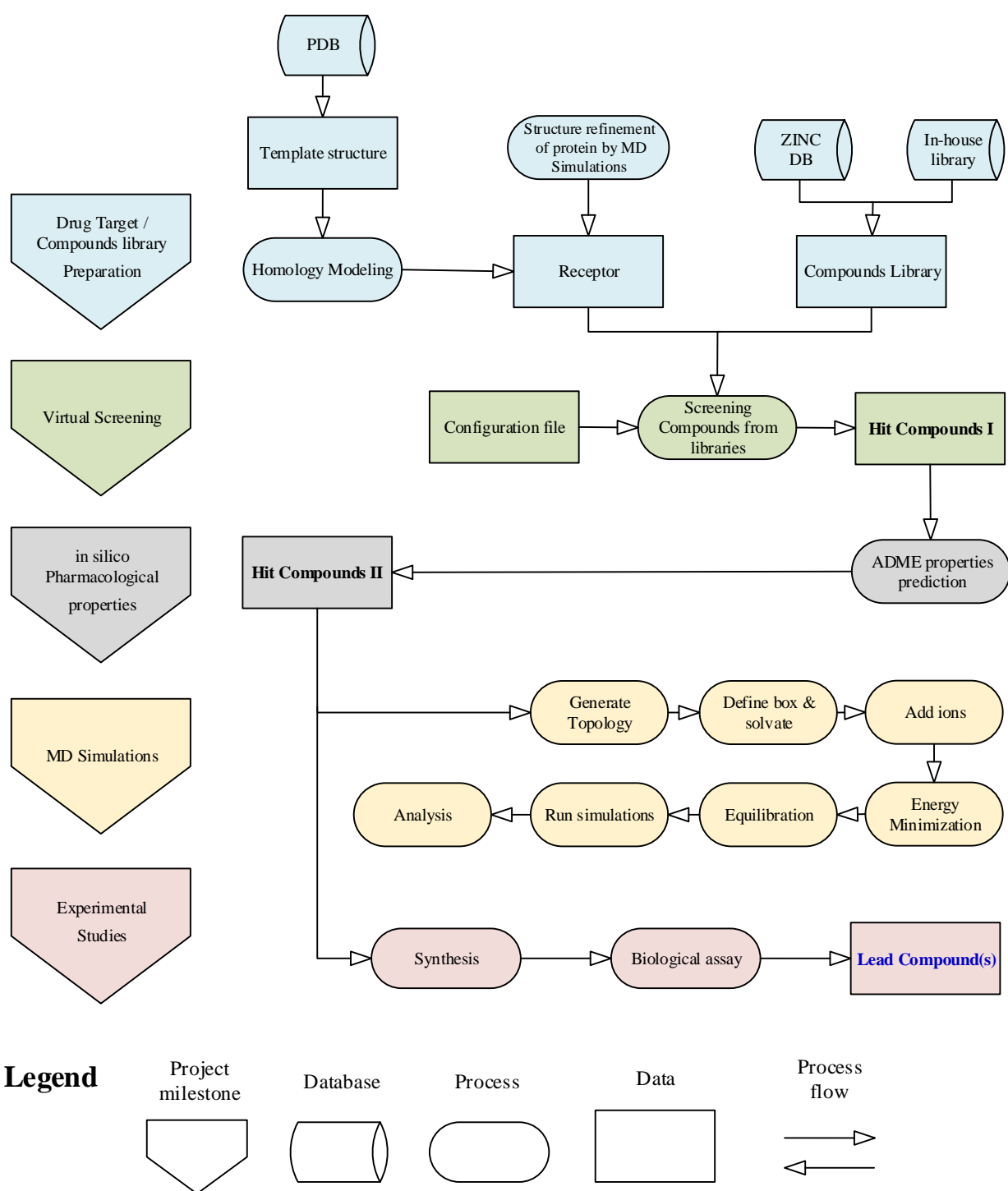
Figure 1. Flowchart of research methodology

To assess the results of virtual screening by USCF DOCK6, MD simulations of top hit compounds were carried out at 100ns. In addition, the hit compounds complexed with the modelled protein were undergone for protein-ligand complex simulations. The topologies of the receptor and each top hit compound were prepared separately and then joined into a single GROMACS file. The system is finally prepared and run after solvation, ionization, energy minimization, and equilibration.

2.1.5. Hardware & Software

The homology model of NS3 protease was used from our previous studies [18,19]. The docking studies were carried out through the Linux operating system (Ubuntu 18.04.5 LTS, x86_64) with remotely accessed virtual machines with a range of processing power. The list of software and hardware used in the study is listed in appendix-A, Table 1 and Table 2.

2.2. Experimental Studies

2.2.1. Organic Synthesis of the Hit Compounds

The chemicals and solvents were purchased from Sigma Aldrich and Alfa Aesar and used for experimental work without further purification. Silica GEL G TLC plates were used to monitor all reactions, and the spots were detected under UV lamps of long and short wavelengths (model UVGL-minor light multiband UV- 254/366). In addition, the purity of synthesized compounds was also checked by using silica gel G TLC plates.

2.2.2. Synthesis Schemes of the Hit Compounds

The synthesis of the hit compounds was performed after the optimization of top compounds obtained after the results of virtual screening. The synthetic scheme of each hit compound is shown in the figures: General synthetic scheme of the hit compounds is given in **Figure 2**. The synthesis of fragments of hit compounds are given in the appendix (Appendix-B, Figure 1 and Table 1).

Synthesis of N-(2-(4-(piperidin-1-ylsulfonyl)benzylamino)ethyl)-N-(2,4,5-trichlorophenyl)methanesulfonamide (TCP)

1-(4-(bromomethyl)phenylsulfonyl)piperidine (0.1749 g) was taken in a round-bottomed flask (150 mL) and dissolved into 5% DMF (15 mL). N-(2-aminoethyl)-N-(2,4,5-trichlorophenyl)methanesulfonamide (0.15 g) was added to it and stirred at room temperature for 8 hours. Lithium hydride (0.002 g) was also added as a catalyst. TLC (hexanes, acetate; 80:20) showed a single spot. The reaction mixture was quenched with chilled water, and the product precipitated, filtered, and dried. The structure and physical properties of the compound are shown in **Figure 3** (a).

Synthesis of N-(2-(4-(morpholinosulfonyl) benzyl amino)ethyl)-N-(2,4,5-trichlorophenyl)methanesulfonamide (TCM)

4-(4-(bromomethyl)phenylsulfonyl)morpholine (0.17375 g) was taken in the round-bottomed flask (150 mL) and dissolved into 5% DMF (15 mL). N-(2-aminoethyl)-N-(2,4,5-trichlorophenyl)methanesulfonamide (0.15 g) was added to it and stirred at room temperature for 8 hours 15 minutes. Lithium hydride (0.002 g) was also added as a catalyst. TLC (hexanes, acetate; 80:20) showed a single spot. The reaction mixture was quenched with chilled water, and the product precipitated, filtered, and dried. The structure and physical properties of the compound are shown in **Figure 3** (b).
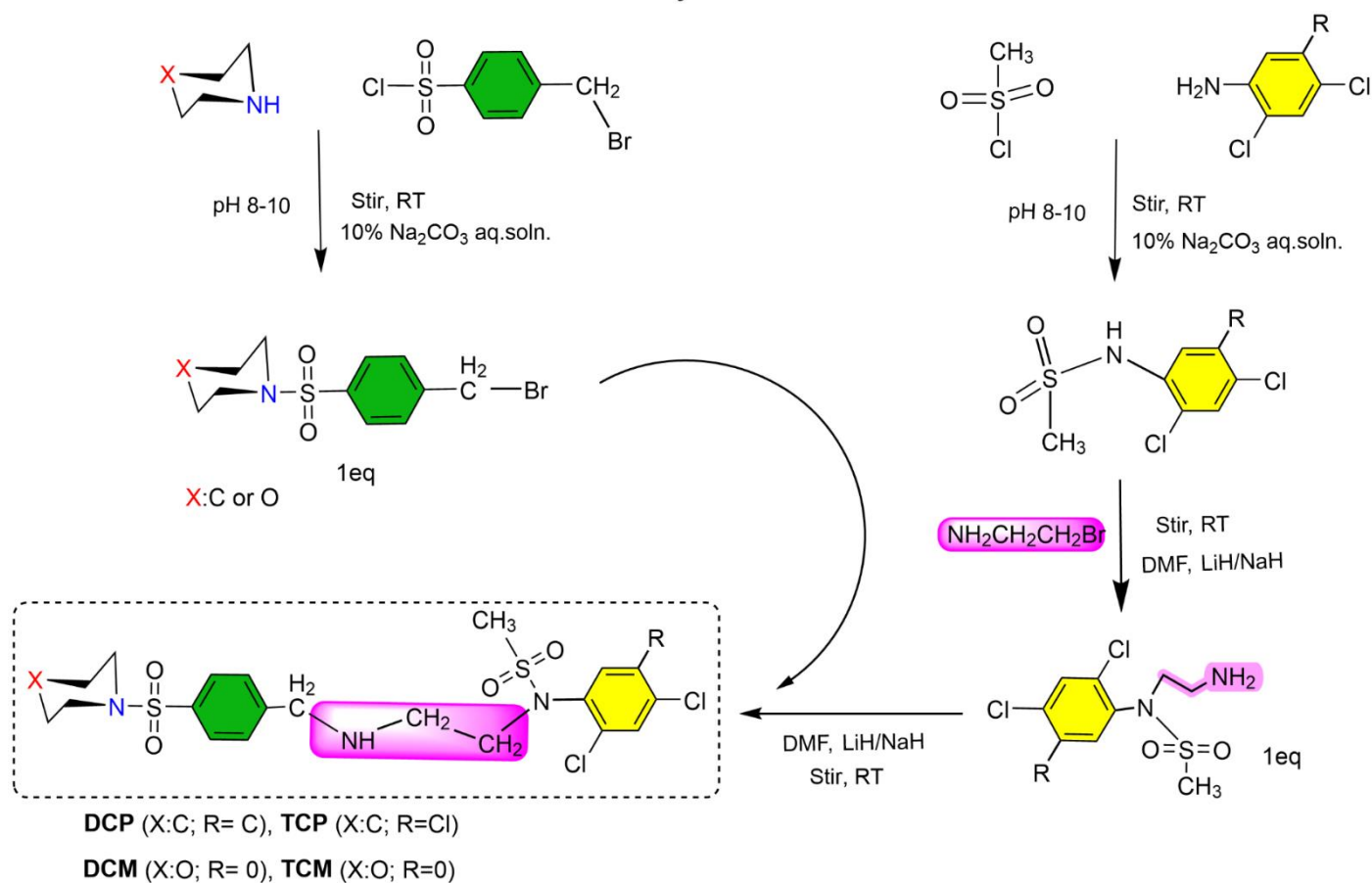
General Synthetic Scheme

Figure 2. General synthetic scheme of the hit compounds.
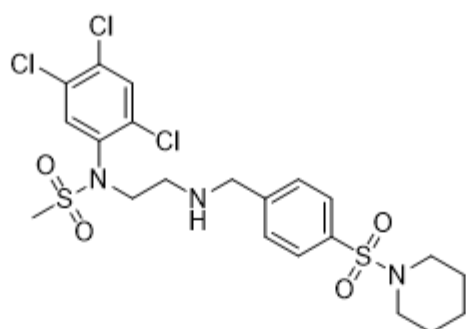
Synthesis of N-(2,4-dichlorophenyl)-N-(2-(4-(piperidin-1-ylsulfonyl)benzyla-mino)ethyl)methanesulfonamide (DCP)

N-(2-aminoethyl)-N-(2,4-dichlorophenyl)methanesulfonamide (0.34 g) was taken in a round-bottomed flask (150 mL) and dissolved into 5% DMF (15 mL). 1-(4-(Bromome-thyl)phenylsulfonyl)piperidine (0.38 g) was added to it and stirred at room temperature for 10 hours. Lithium hydride (0.002 g) was also added as a catalyst. TLC (hexanes, acetate; 80:20) showed a single spot. The reaction mixture was quenched with chilled water, and the product precipitated, filtered, and dried. The structure and physical properties of the compound are shown in **Figure 3** (c).

Synthesis of N-(2,4-chlorophenyl)-N-(2-(4-(morpholinosulfonyl)benzyla-mine)ethyl)methanesulfonamide (DCM)
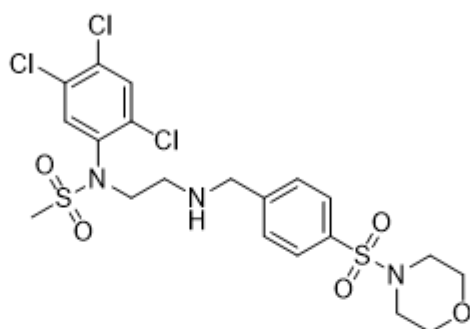
N-(2-aminoethyl)-N-(2,4-chlorophenyl)methanesulfonamide (0.35 g) was taken in the round-bottomed flask (150 mL) and dissolved into 5% DMF (15 mL). 4-(4-(Bromome-thyl)phenylsulfonyl)morpholine (0.4 g) was added to it and stirred at room temperature for 6 hours. Lithium hydride (0.002 g) was also added as a catalyst. TLC (hexanes, acetate; 80:20) showed a single spot. The reaction mixture was quenched with chilled water, and the product precipitated, filtered, and dried. The structure and physical properties of the compound are shown in **Figure 3** (d).
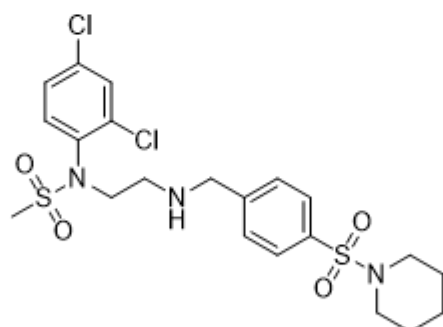
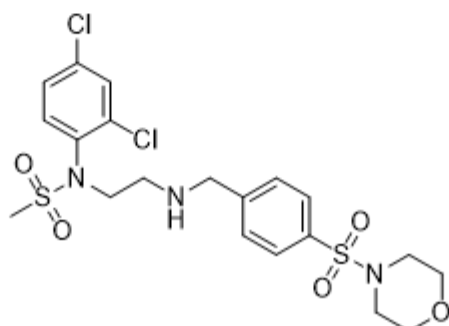N-(2-(4-(piperidin-1-ylsulfonyl)benzylamino)ethyl)-N-(2,4,5-trichlorophenyl)methanesulfonamide

N-(2-(4-(morpholinosulfonyl)benzylamino)ethyl)-N-(2,4,5-trichlorophenyl)methanesulfonamide

N-(2,4-dichlorophenyl)-N-(2-((4-(piperidin-1-ylsulfonyl)benzyl)amino)ethyl)methanesulfonamide

N-(2,4-dichlorophenyl)-N-(2-((4-(morpholinosulfonyl)benzyl)amino)ethyl)methanesulfonamide

Figure 3. Structures of the compounds TCM (a), TCP (b), DCP (c), DCM (d).

2.3. Biological Evaluations

2.3.1. Cell Culture

HGF and AGS Culture

A total of 10 healthy donors, undergone to third molars extraction, signed the informed consent according to the Italian Law and to the Ethical Principles for Medical Research code including Human Subjects of the World Medical Association (Declaration of Helsinki). The project was approved by the Local Ethical Committee of the University of Chieti (Chieti, Italy, approval number. 1173, approved on 31/03/2016). Gingiva biopsies were rinsed in phosphate-buffered saline (PBS), placed in Dulbecco's modified Eagle's medium (DMEM), cut into smaller pieces and cultured in DMEM, with 10% foetal bovine serum (FBS), 1% penicillin/streptomycin and 1% fungizone (all purchased from Merck Life Science, Milan, Italy). After 10 days of culture, fungizone was removed from the medium and cells cultured until 5-8 passages. AGS human gastric adenocarcinoma cell line (ECACC 89090402, Merck Life Science, Milan, Italy) was cultured in Ham's F12 medium with 10% of FBS, 1% of penicillin/streptomycin, and 1% of L−glutamine (all purchased from Merck Life Science). Both cell cultures were maintained at 37 °C within an incubator in presence of 5% (v/v) CO_2.

HGF and AGS Treatment

For each compound, a stock solution 0.1 M was prepared using DMSO as vehicle. Then, the stock solution was diluted in DMEM or Ham's F12 medium (for HGFs and AGS, respectively) to obtain intermediate solutions of 100 µM and final solutions of 50 and 10 µM for HGFs and of 50 µM for AGS. To exclude DMSO cytotoxicity, the final concentration of DMSO within the culture medium was kept at 0.05%.

The HGFs and AGS cells were seeded at 6700 and 8000 cells/well, in a 96 multiwell plate, respectively. After 24 h from seeding, the medium (DMEM and Ham's for HGFs and AGS, respectively) was replaced by a fresh one containing compounds at 10 and 50 µM for HGFs. In AGS culture newly synthesized compounds were administered at 50 µM. Treatments were maintained from 48 to 72 h within an incubator in a humified atmosphere in presence of 5% (v/v) CO_2 at 37 °C.

2.3.2. MTT Metabolic Activity test

After 48 and 72 h of culture an MTT (3−(4,5−dimethylthiazol−2−yl)−2,5−diphenyltetrazolium bromide) assay was carried out. The MTT test measures the viable cells capability to transform MTT into a violet formazan salt. At the established experimental time points, the culture medium was added of MTT 10% (Merck Life Science, Milan, Italy) and incubated at 37 °C for 5 h for HGFs and for 4 h (for AGS). To dissolve formazan salts plate was probed in DMSO for 30 min at 37 °C, then read at 540 nm wavelength through a microplate reader (Multiskan GO, Thermo Scientific, Waltham, MA, USA). The obtained values were normalized with values derived from cells treated with DMSO (vehicle).

2.3.3. Statistics

Statistical analysis was performed using the GraphPad 7 software (GraphPad Software, San Diego, CA, USA) by means of Ordinary One−Way ANOVA followed by post−hoc Tukey's multiple comparison tests.

2.3.4. SPR Assay

The purified DNA sequence encoding the Hepatitis C virus (HCV)(serotype 1a, isolate H77) NS3 (NP_803144.1) (Thr1356-Thr1459) was expressed with a GST tag at the N-terminus was purchased from Sino Biological enzyme was immobilized on flow channels 2 and 4 of a CM5 sensor chip using modified GST-coupling with running buffer HBS-EP (10 mM HEPES, 150 mM NaCl, 0.05% surfactant P-20, pH 7.4) using a Biacore S200 instrument. Flow channels 1 and 3 were used as control surfaces. The HCV-NS3 enzyme was diluted in 10 mM sodium acetate (pH 5.0) and immobilized after sensor surface activation with 1-ethyl-3-(3-dimethylaminopropyl)carbodiimide hydrochloride (EDC)/N-hydroxy succinimide (NHS) mixture followed by ethanolamine (pH 8.5) blocking on unoccupied surface area.

The selected compound was initially prepared as 10 mM DMSO stock solutions, and compound solutions with a series of increasing concentrations (2.4-1500 5-fold dilution) were applied to all four channels at a 30 μL/min flow rate at 25 °C. Sensorgrams were analyzed using BIAevaluation software 3.0, and response unit difference (ΔRU) values at each concentration were measured during the equilibrium phase. All data were double referenced with both blank surface and zero compound concentration responses and fitted with steady-state affinity equation (equation 14) where y is the response, Ymax is the maximum response and x is the compound concentration [53]. Refer to appendix E for pH scouting.

$$y = \frac{y_{max} \cdot x}{(K_D + x)}$$

3. Results and Discussion

3.1. Computational Studies

3.1.1. Virtual Screening of One Million ZINC Library Compounds

One million compounds retrieved from the ZINC database were screened against modelled NS3 protease GT 3a Using UCSF DOCK6. Due to computational resource constraints, the whole compound library of one million compounds was subjected to rigid docking on remote virtual servers. The scheme of the virtual screening is given below. Initially, the top 4000 compounds with better grid scores were selected and redocked again to shortlist the top 1000 compounds. Onward, these compounds were kept on docking through flexible docking (anchor and grow algorithm) until the top nine compounds were come out as hit compounds (**Figure 4**). Finally, the top nine compounds were selected having grid scores greater than -53. The attributes of these top compounds, such as rotatable bonds, molecular weight, electrostatic interaction energy, and repulsive energy, were noted and compared (**Table 1**). The ZINC ID of the selected hit compounds are ZINC000100685029, ZINC000005273907, ZINC000003917816, ZINC000101149671, ZINC000101574832, ZINC000224822442, ZINC000224449889, ZINC000224374291, and ZINC000224374456.
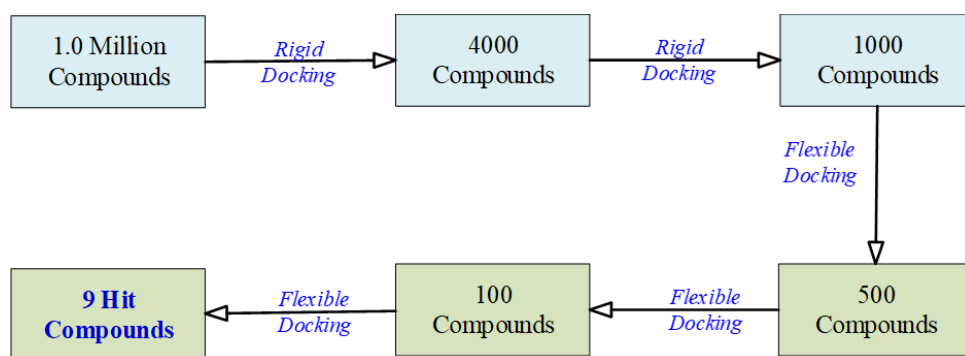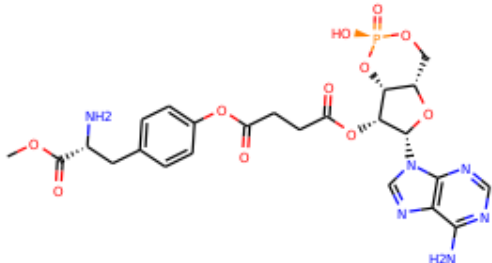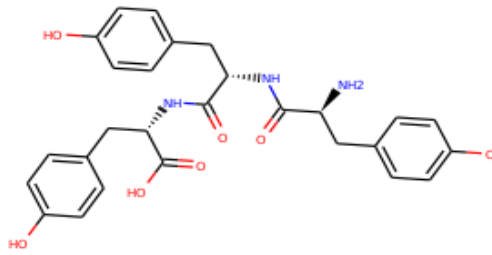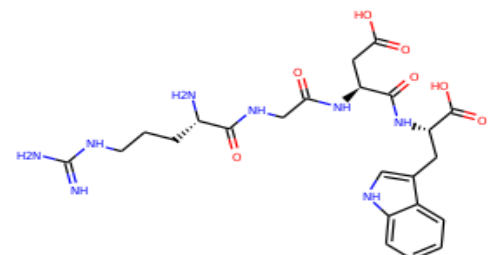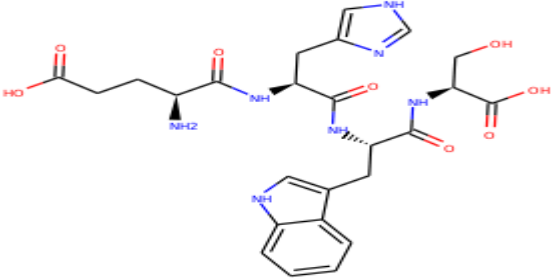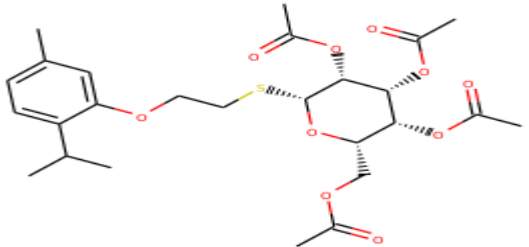

Figure 4. Workflow of virtual screening.

Table 1. Virtual Screening results and pharmacokinetics studies of top hit compounds. Pharmacokinetics Studies of the top compounds. The pharmacokinetics parameters are defined beneath the table.

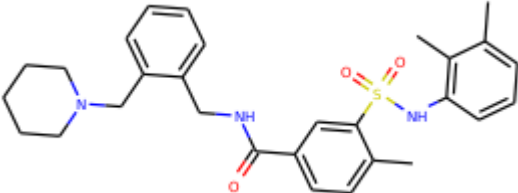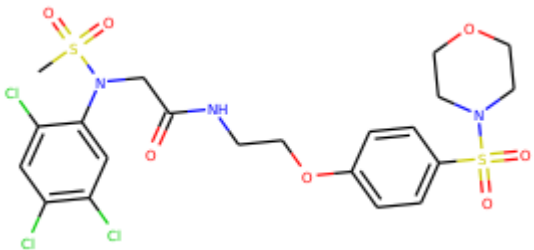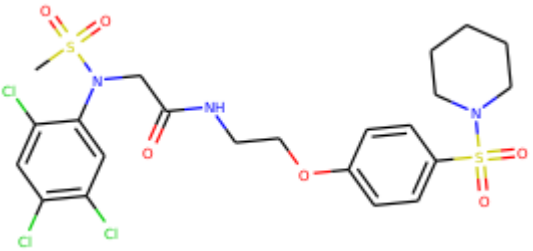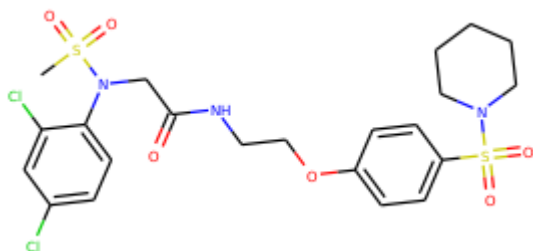| S.No.	Molecule ID	Structure	DOCK 6 Results	Molecular Properties
1	ZINC000100685029		Grid Score: -62.41 DOCK Rotatable Bonds: 12 Molecular Weight: 606.48 Formal Charge: 0.010 Grid VDW Energy: -48.31 Grid ES Energy: -14.10 Internal Energy Repulsive: 17.97	miLogP: -1.11 TPSA: 239.57 natoms: 42 MW: 606.49 nON: 17 nOHNH: 5 nrotb: 12 volume: 488.37
2	ZINC000005273907		Grid Score: -59.34 DOCK Rotatable Bonds: 16 Molecular Weight: 507.54 Formal Charge: 0.02 Grid VDW Energy: -47.01 Grid ES Energy: -12.32 Internal Energy Repulsive: 15.78	miLogP: -0.87 TPSA: 182.20 natoms: 37 MW: 507.54 nON: 10 nOHNH: 8 nrotb: 11 volume: 452.86
3	ZINC000003917816		Grid Score: -58.56 DOCK Rotatable Bonds: 19 Molecular Weight: 532.55 Formal Charge: -6.70e-07 Grid VDW energy: -46.64 Grid ES energy: -11.92 Internal energy repulsive: 17.74	miLogP: -4.31 TPSA: 265.61 natoms: 38 MW: 532.56 nON: 15 nOHNH: 12 nrotb: 16 volume: 469.75

4	ZINC000101149671		Grid Score: -56.99 DOCK Rotatable Bonds: 19 Molecular Weight: 557.56 Formal Charge: 0.01 Grid VDW Energy: -48.16 Grid ES Energy: -8.83 Internal Energy Repulsive: 15.16	miLogP: -4.48 TPSA: 252.62 natoms: 40 MW: 557.56 nON: 15 nOHNH: 10 nrotb: 15 volume: 484.05
5	ZINC000101574832		Grid Score: -56.18 DOCK Rotatable Bonds: 15 Molecular Weight: 540.63 Formal Charge: -0.02 Grid VDW Energy: -51.30 Grid ES Energy: -4.88 Internal energy repulsive: 33.20	miLogP: 3.99 TPSA: 123.69 natoms: 37 MW: 540.63 nON: 10 nOHNH: 0 nrotb: 15 volume: 488.47
6	ZINC000224822442		Grid Score: -54.43 DOCK Rotatable Bonds: 9 Molecular Weight: 505.68 Formal Charge: -0.02 Grid VDW Energy: -47.58 Grid ES Energy: -6.85 Internal Energy Repulsive: 37.15	miLogP: 5.14 TPSA: 78.50 natoms: 36 MW: 505.68 nON: 6 nOHNH: 2 nrotb: 8 volume: 471.32

7	ZINC000224449889		Grid Score: -54.12	miLogP: 3.75
			DOCK Rotatable Bonds: 11	TPSA: 122.33
			Molecular Weight: 600.92	natoms: 36
			Formal Charge: 0.03	MW: 600.93
			Grid VDW Energy: -53.63	nON: 10
			Grid ES Energy: -0.48	nOHNH: 1
			Internal Energy Repulsive: 17.71	nrotb: 10
				volume: 457.18
8	ZINC000224374291		Grid Score: -53.86	miLogP: 4.82
			DOCK Rotatable Bonds: 11	TPSA: 113.09
			Molecular Weight: 598.95	natoms: 36
			Formal Charge: 0.009	MW: 598.96
			Grid VDW Energy: -53.50	nON: 9
			Grid ES Energy: -0.35	nOHNH: 1
			Internal Energy Repulsive: 16.58	nrotb: 10
				volume: 464.99
9	ZINC000224374456		Grid Score: -53.38	miLogP: 4.21
			DOCK Rotatable Bonds: 11	TPSA: 113.09
			Molecular Weight: 564.51	Natoms: 35
			Formal Charge: -1.49e-07	MW: 564.51
			Grid VDW Energy: -51.35	nON: 9
			Grid ES Energy: -2.03	nOHNH: 1
			Internal Energy Repulsive: 45.04	nrotb: 10
				volume: 451.46

337
338

milogP: LogP (octanol/water partition coefficient)   TPSA: Molecular Polar Surface Area

MW: Molecular Weight   nON: number of Hydrogen bond acceptors

nOHNH: number of Hydrogen bond donors   nrotb: Number of Rotatable Bonds

339
340

3.1.2. Pharmacokinetics Studies of Top Hit Compounds

The physicochemical parameters related to drug-likeness, adsorption, distribution, metabolism, and excretion (ADME) were calculated for the top hit compounds using molinspiration to assess their pharmacokinetics properties (**Table 1**).

All the hit compounds conform to the molinspiration parameter except for a few deviations. The compounds ZINC000100685029, ZINC000005273907, ZINC000003917816, ZINC000101149671, ZINC000101574832, and ZINC000224822442 have slightly more hydrophobicity which affects drug absorption, bioavailability, hydrophobic drug-receptor interactions, metabolism of molecules, as well as their toxicity (**Table 1**). The remaining three compounds, ZINC000224449889, ZINC000224374291, and ZINC000224374456, demonstrated favorable properties to conform with the Lipinski rule of 5. However, the molecular volume of the latter is a little bit high, which is also essential to occupy the wide binding site of NS3 protease.

Thus, the ADME studies showed that compounds ZINC000224449889, ZINC000224374291, and ZINC000224374456 exhibited good pharmacokinetic properties and therefore taken for further experimental studies to validate the theoretical study's findings.

3.2. *Crystal Structure of HCV NS3 Protease*

At the time of synopsis approval from the Board of Advance Studies and Research (BASR) dated 23rd April 2019, the crystal structure of HCV NS3 protease GT3a was not yet revealed. So, the homology model of HCV NS3 protease GT3a was constructed using SwissDock for computational studies.

However, its structure was resolved by Timm, J. et al. and released by Protein Data-Bank on 10th Jun 2020 with PDB ID: 6P6S. However, its paper is not published to date. So, it became incumbent to compare the results with the crystal structure obtained against the modelled structure of NS3 protease. Hence, the structure and the docking results against the modelled protein were compared with the crystal structure.

3.2.1. Comparison of Crystal Structure with the Modelled Protein

The 3D conformation of modelled NS3 protease and the recently reported crystal structure (PDB entry: 6P6S) exhibited similar coordinates, with an RMSD difference of 0.610 Å (**Figure 5**). Furthermore, the sequence alignment of both proteins resulted in 100% sequence identity with an E-value of 2e-145.

The top hit compounds were also docked against the crystal structure of NS3 protease. The seven clinically validated reported compounds were also taken into consideration to assess the difference between the results of both proteins and the variation in results between the hit and the reported compounds (**Table 2**). Interestingly, under the same parameters, most of the hit compounds and the reported compounds exhibited better grid scores in the case of the modelled protein than that of the crystal structure. Except for a single compound, ZINC000101149671, the rest of the hit compounds exhibited a better grid score against the modelled protein than the crystal structure. Similarly, the clinically reported compounds, Telaprevir, Voxilaprevir, and Simeprevir, demonstrated a better grid score, i.e., -50.90, -60.29, and -59.09 respectively, against the modelled protein compared to -49.79, -42.60, and -45.89 in the same order against the crystal structure. The compound Paritaprevir has almost the same grid score against both proteins (**Table 2**). Thus, the compound with a better grid score will have better binding with the target protein and better inhibitory potential. Furthermore, when the hit compounds and the clinically validated compounds (control) are compared, most of the hit compounds revealed better grid scores than the control compounds. In fact, the reported compounds, Glecaprevir (-26.46), Grazoprevir (-46.85), and Boceprevir (-34.73), showed even low grid scores than the hit compound with the least grid score i.e., -53.38 (**Table 2**).

For more detailed comparison, the top two hit compounds ZINC000224374291 and ZINC000224374456, are shown as docked poses into the active site of the modelled and

template protein overlapping each other (**Figure 6**). The docking score and intermolecular interaction of both compounds are given in detail in **Table 3** and shown in **Figure 6**. The catalytic triad residues, His57, Asp81 and Ser139, are predominant in the active site of both proteins along with binding groove residues, especially Arg155 and Ala156. The compound ZINC000224374291 makes three hydrogen bonds and three electrostatic interactions with the modelled protein as well as crystal structure protein. The residues that are involved in hydrogen bonding are His57 (3.87 Å), Asp81 (5.00 Å) and Arg155 (2.87 Å) with the modelled protein. Similarly, the same residues form hydrogen bond with the crystal protein with the bond length 5.00 Å, 5.21 Å and 2.95 respectively. In the case of the compound, ZINC000224374456, three are three hydrogen bonds with the modelled protein and two bonds with the crystal structure protein. His57 is the dominant residues involved in hydrogen bonds. Ser139 and Ala156 of modelled protein are predominant in electrostatic interactions whereas Ser139 and Arg155 are major residues involved in electrostatic interactions in case of crystal protein. The residue Leu135 is mainly responsible for Van der Waals interactions for both the protein (**Table 3**, **Figure 6**).

Table 2. Docking Score results of the modelled and crystal proteins.

| Molecule ID / Name	DOCK6 Score of Modelled NS3 GT3	DOCK6 Score of NS3 Crystal Structure
ZINC000100685029	-62.41	-59.62
ZINC000005273907	-59.34	-52.02
ZINC000003917816	-58.56	-63.77
ZINC000101149671	-56.99	-58.79
ZINC000101574832	-56.18	-50.33
ZINC000224822442	-54.43	-48.15
ZINC000224449889	-54.12	-48.30
ZINC000224374291	-53.86	-50.07
ZINC000224374456	-53.38	-50.13
Paritaprevir	-55.25	-55.62
Glecaprevir	-26.46	-44.46
Grazoprevir	-46.85	-64.67
Telaprevir	-50.90	-49.79
Voxilaprevir	-60.29	-42.60
Simeprevir	-59.09	-45.89
Boceprevir	-34.73	-46.79
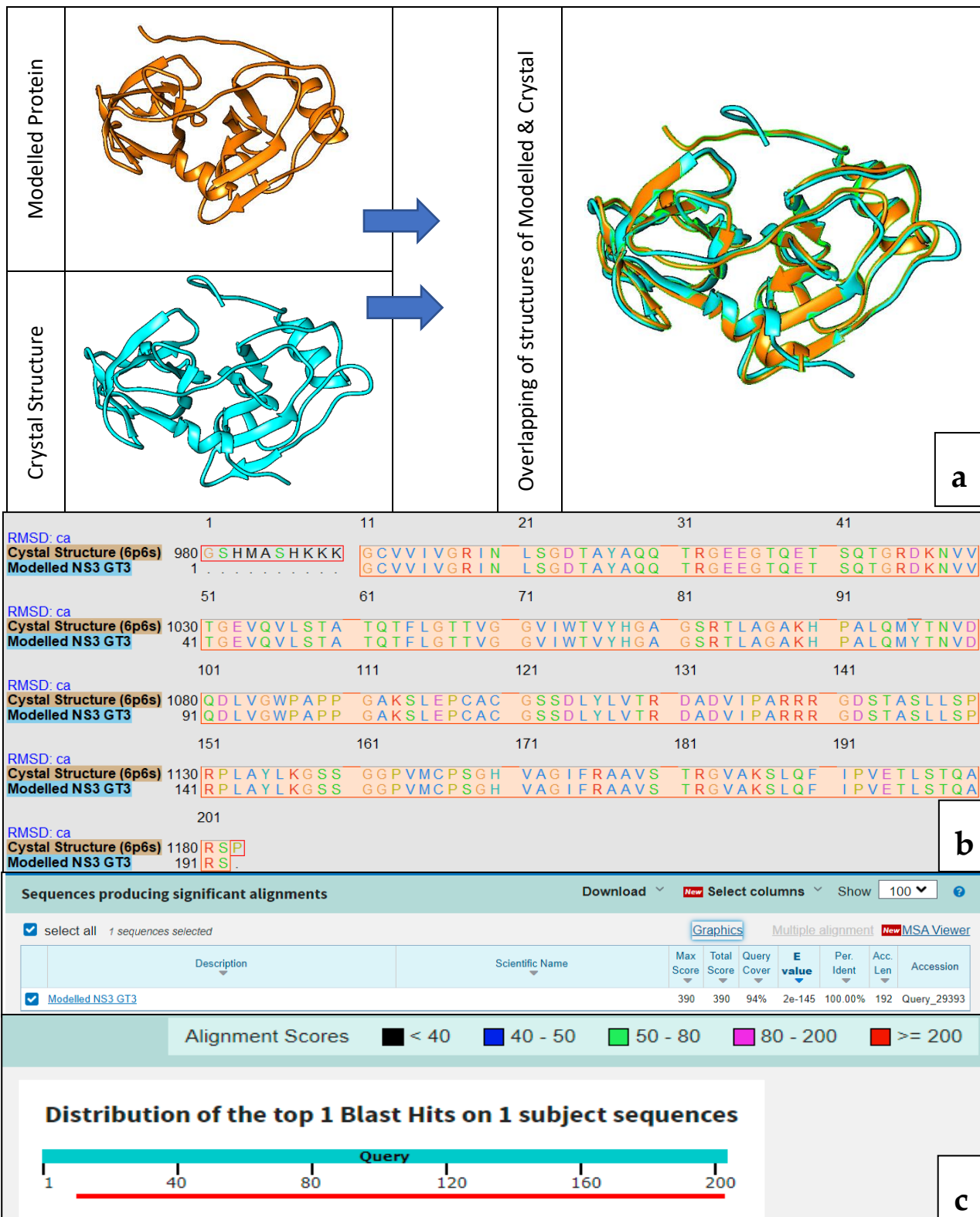
Figure 5. Comparison between the modelled (orange) and the crystal structure (cyan) of NS3 protease.
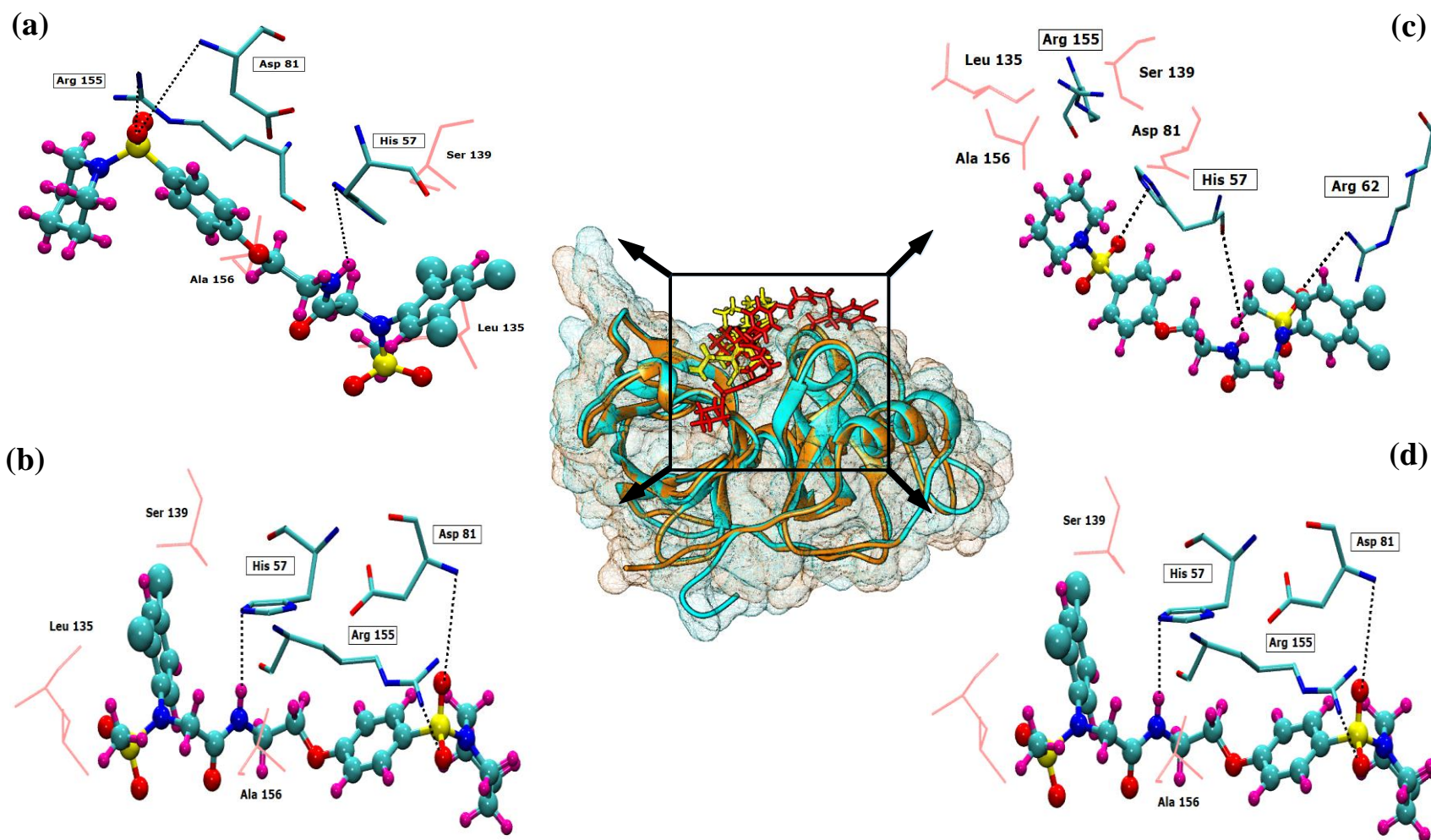
Figure 6. The modelled protein (orange) and the crystal protein (cyan) are overlapped surrounded by meshed surface of both proteins in respective colors (center). The docked pose of the hit compound ZINC000224374291 and ZINC000224374456 for the modelled protein (yellow) and the crystal protein (red) are shown on the binding groove of the overlapped proteins. The interaction images of ZINC000224374291 (a) and ZINC000224374456 (b) with the modelled protein are given. Similarly, interaction images of both the compounds i.e., ZINC000224374291 (c) and ZINC000224374456 (d), are shown in complex with the crystal protein.

Table 3. Proteins Ligand Interactions of NS3 Modelled Structure and Crystal Structure.

	Molecule ID	DOCK6 Score		Hydrogen Bonds	Electrostatic Interactions	Vdw interactions
Modelled Protein	ZINC000224374291	Grid Score: Grid VDW Energy: Grid ES Energy: Internal Energy Repulsive:	-53.86 -53.50 -0.35 16.58	His57 with amino group (3.87 Å) Arg155 with sulfonamide (2.78 Å)	Ser139 with trichloro-benzene ring Ala156 with carbonyl group	Leu135 with trichloro-benzene ring
	ZINC000224374456	Grid Score: Grid VDW Energy: Grid ES Energy: Internal Energy Repulsive:	-53.38 -51.35 -2.03 45.04	His57 with amino group (2.82 Å) Asp81 with sulfonamide (3.76 Å) Arg155 with sulfonamide (2.59 Å)	Ser139 with trichloro-benzene ring Ala156 with carbonyl group	Leu135 with trichloro-benzene ring
Crystal Protein	ZINC000224374291	Grid Score: Grid VDW Energy: Grid ES Energy: Internal Energy Repulsive:	-50.07 -45.42 -4.65 20.09	Arg62 with sulfonamide (2.95 Å)	Ser139 with sulfonamide adjacent to piperidine ring Arg155 with sulfonamide adjacent to piperidine ring	Leu135 with piperidine ring Ala156 with piperidine ring
	ZINC000224374456	Grid Score: Grid VDW Energy: Grid ES Energy: Internal Energy Repulsive:	-50.13 -44.66 -5.46 23.90	His57 with sulfonamide (3.02 Å) Ala133 with sulfonamide (2.95 Å)	Ser139 with sulfonamide adjacent to piperidine ring Arg155 with sulfonamide adjacent to piperidine ring	Leu135 with piperidine ring Ala156 with piperidine ring

3.3. Experimental Studies   426

3.3.1. Synthesis and Optimization of the Hit Compounds   427

   Given the favorable results from virtual screening and in-silico pharmacokinetic   428
studies, the compounds ZINC000224449889, ZINC000224374291, and ZINC000224374456   429
have grid scores Grid Score -54.12, -53.86, and -53.38 were selected as the hit compounds   430
for organic synthesis. The position and number of chlorines on the benzene ring and at-   431
tachment of morpholine or piperidine rings through the linker embodies the difference   432
between the hit compounds. However, the bulky linker (highlighted in the table below)   433
was reoptimized and shortened for better organic synthesis viability. As a result, the hit   434
ZINC compounds were modified for optimized organic synthesis (**Table 4**). To keep the   435
hit compounds' name simple and meaningful, the compound ZINC000224449889 was re-   436
named Trichloromorpholine abbreviated as TCM having three chlorines attached to the   437
benzene ring and morpholine attached to it through the linker. Similarly, the other com-   438
pounds ZINC000224374291 and ZINC000224374456 were renamed Trichloropiperidine   439
(TCP) and Dichloropiperidine (DCP), respectively. To check the effect of morpholine moi-   440
ety with the DCM, an additional compound was synthesized as Dichloromorpholine   441
(DCM), replacing piperidine with morpholine.   442

   The modified compounds were re-evaluated against the modelled receptor and the   443
crystal structure by performing their molecular docking, keeping the same parameters   444
and conditions set for the hit compounds (**Table 5**). Additionally, Root Mean Square Fluc-   445
tuation (RMSF) of the optimized compounds was calculated through MD simulations in   446
case of the modelled NS3 protease to further assess its flexibility in bound (complex with   447
the hit compounds) and non-bound (single protein) (**Figure 7**). The simulations results   448
exhibit overall compactness in bound and non-bound form. More fluctuations were ob-   449
served between the protein and compound DMC from atoms 300 to 600 and terminal res-   450
idues in case of compound DCP.   451

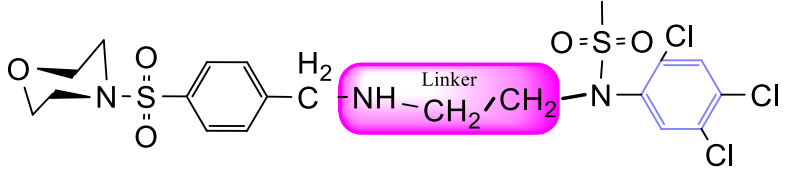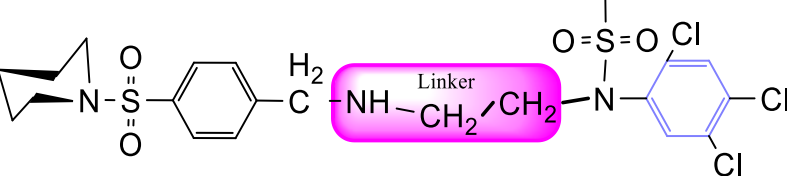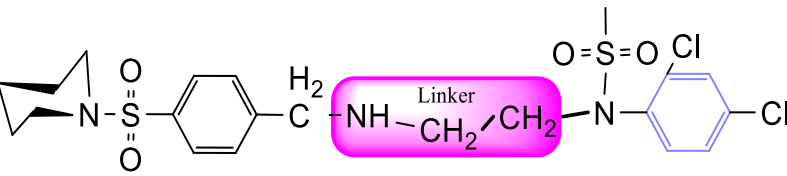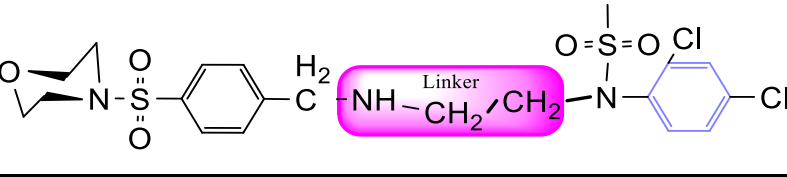   452

Table 4. Organic synthesis of the hit compounds.

| ZINC ID	Modified Compound Name	Compound Code	Compound Structure
ZINC000224449889	N-(2-(4-(morpholinosulfonyl)benzylamino)ethyl)-N-(2,4,5-trichlorophenyl)methanesulfonamide	TCM	
ZINC000224374291	N-(2-(4-(piperidin-1-ylsulfonyl)benzylamino)ethyl)-N-(2,4,5-trichlorophenyl)methanesulfonamide	TCP	
ZINC000224374456	N-(2,4-dichlorophenyl)-N-(2-(4-(piperidin-1-ylsulfonyl)benzylamino)ethyl)methanesulfonamide	DCP	
Derivative of DCP	N-(2,4-dichlorophenyl)-N-(2-(4-(morpholinosulfonyl)benzylamino)ethyl)methanesulfonamide	DCM	
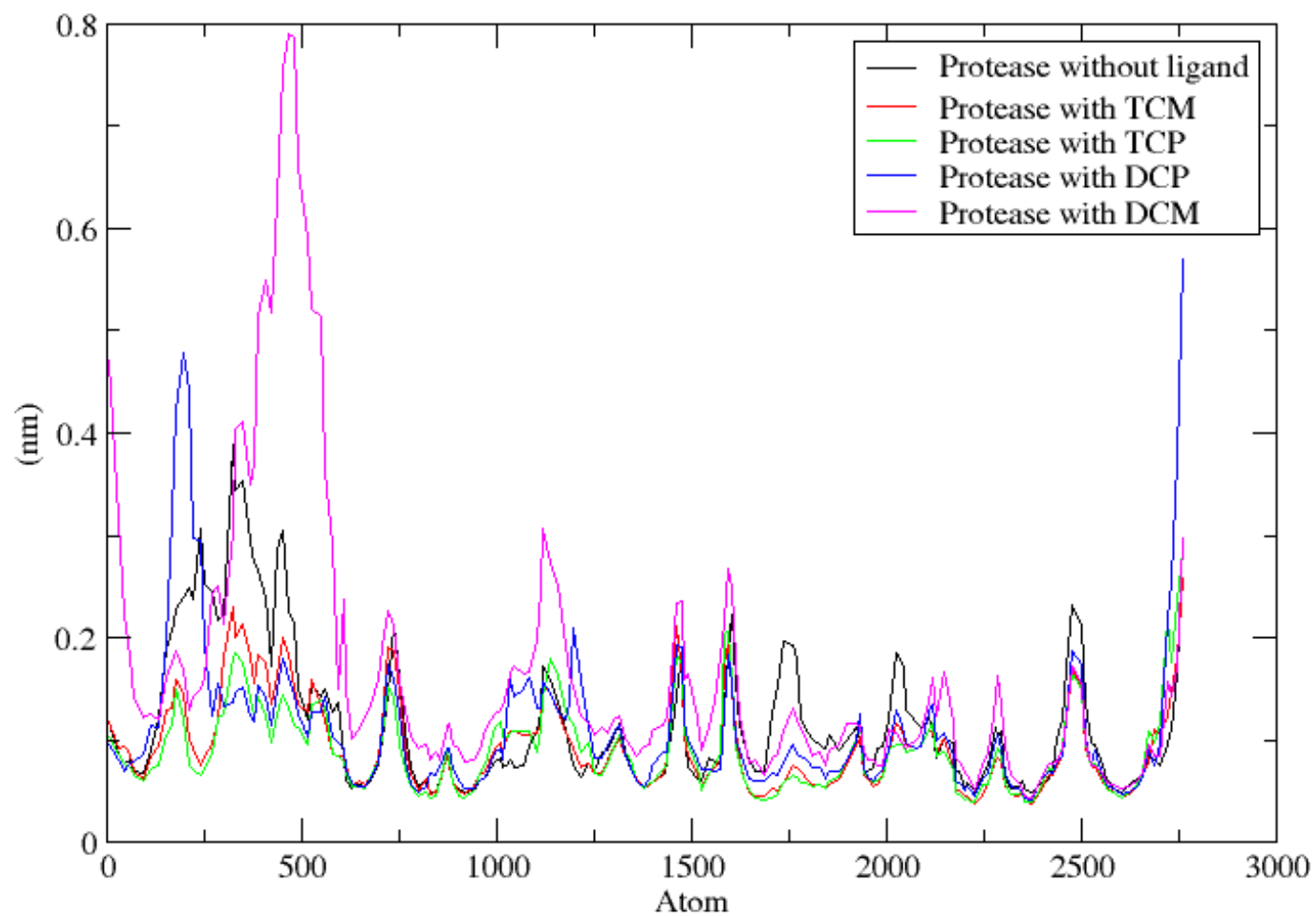
Figure 7. RMSF analysis of NS3 protease in bound and non-bound form. The peaks of NS3 protease (black), The hit compounds, TCM (red), TCP (green), DCP (blue) and DCM (magenta) are shown.

Table 5. Docking score of the synthesized organic compounds

Compound Code	DOCK6 Score of Modelled NS3 GT3	DOCK6 Score of NS3 Crystal Structure
TCM	Grid Score: -42.36 Grid VDW Energy: -41.97 Grid ES Energy: -0.39 Internal Energy Repulsive: 14.18	Grid Score: -45.45 Grid VDW Energy: -45.06 Grid ES Energy: -0.39 Internal Energy Repulsive: 10.30
TCP	Grid Score: -43.11 Grid VDW Energy: -42.14 Grid ES Energy: -0.97 Internal Energy Repulsive: 10.46	Grid Score: -43.89 Grid VDW Energy: -42.94 Grid ES Energy: -0.94 Internal Energy Repulsive: 13.30
DCP	Grid Score: -46.88 Grid VDW Energy: -46.43 Grid ES Energy: -0.45 Internal Energy Repulsive: 13.60	Grid Score: -43.11 Grid VDW Energy: -42.43 Grid ES Energy: -0.68 Internal Energy Repulsive: 18.54
DCM	Grid Score: -45.77 Grid VDW Energy: -45.62 Grid ES Energy: -0.14 Internal Energy Repulsive: 14.86	Grid Score: -42.99 Grid VDW Energy: -42.35 Grid ES Energy: -0.63 Internal Energy Repulsive: 13.14

3.3.2. Characterization data of the Hit Compounds and their Corresponding Fragments

All four hit compounds (TCP, DCP, TCM, DCM) were purified by flash chromatography. Compounds were purified with a RediSep Rf Gold Silica Gel Disposable Flash column from Teledyne Isco (4 g, 18 mL/min from rate) with a gradient of EtOAc in hexanes of 0-100% in 7 min, eluting at 35% EtOAc with a 24–39% yield over 3 steps.

3.3.2.1.   N-(2,4-dichlorophenyl)-N-(2-((4-(morpholinosulfonyl)benzyl)amino)ethyl)methane sulfonamide (DCM)
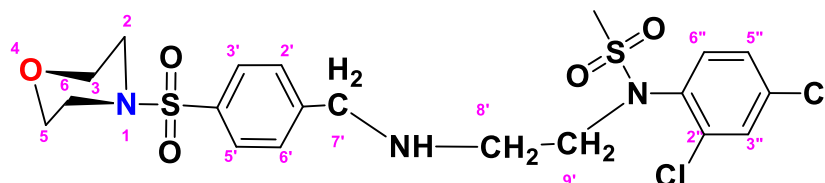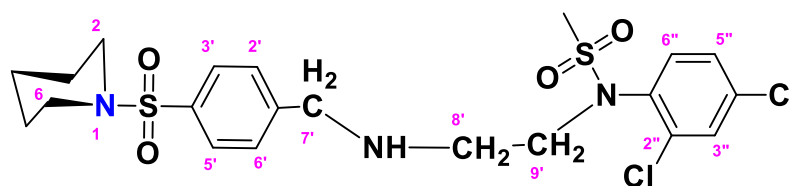

The structure of DCM with the formula $C_{20}H_{25}Cl_2N_3O_5S_2$ is given above. It is solid, white in color, having a molecular weight of 520.49 g/mol, a melting point of 125 °C, and is soluble in DMSO and chloroform. IR (cm^{-1}) V_{max}: 3256 (N-H), 2810 (Ar-H), 1336 (SO$_2$ stretching), 1163 (C-N stretching), 1091 (C-O stretching); HRMS (m/z): [M+1] 522.46 (13%), 522.06 (24%), 281.98 (68%), 240.07 (73%), 147.97 (64%), 91.05 (100.0%). Anal. Calcd: C, 45.98; H, 4.82; N, 8.04; S, 12.27. Found: C, 46.02; H, 4.85; N, 8.06; S, 12.30. ^{1}H NMR (400 MHz, Acetone) δ 7.73–7.49 (m, 2H, H-3' & H-5'), 7.43 (dd, 1H, J = 8.3, 0.5 Hz, H-6''), 7.35 (d, J = 2.4 Hz, 1H, H-3''), 7.17 (dd, J = 8.6, 2.4 Hz, 2H, H-2' and H-6'), 6.98 (d, J = 8.6 Hz, 1H, H-5''), 3.92 (q, J = 7.1 Hz, 2H, CH$_2$-9'), 3.60–3.43 (m, 4H, H-3, H-5), 2.77–2.70 (m, 4H, H-2 and H-6), 1.92 (dq, J = 4.5, 2.3 Hz, 2H, CH$_2$-7'), 1.83 (s, 3H, CH$_3$), 1.06 (t, J = 7.1 Hz, 2H, CH$_2$-8'). The spectra of DCM are given in appendix D.

3.3.2.2.   N-(2-((4-(morpholinosulfonyl)benzyl)amino)ethyl)-N-(2,4,5-trichlorophenyl)methane sulfonamide (TCM)
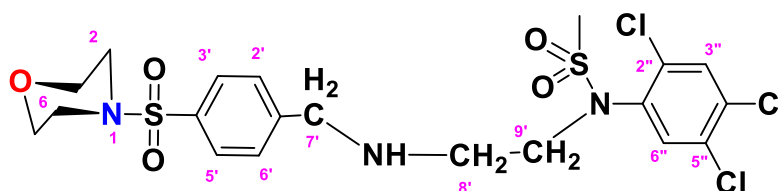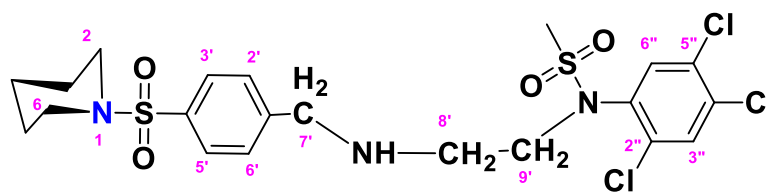

The fragment TCM with the formula $C_{20}H_{24}Cl_3N_3O_5S_2$ is given above. It is solid, brown in color, having a molecular weight of 522.47 g/mol, a melting point of 95 °C, and is soluble in DMSO and chloroform. IR (cm^{-1}) V_{max}: 3251 (N-H), 2809 (Ar-H), 1337 (SO$_2$ stretching), 1168 (C-N stretching), 1085 (C-O stretching); HRMS (m/z): [M+] 556.90 (13.0%), 315.60 (98%), 319.94 (3.5%), 240.07 (73%), 147.97 (64%), 91.05 (100.0%). Anal. Calcd: C, 43.13; H, 4.34; N, 7.55; S, 11.52. Found: C, 43.16; H, 4.37; N, 7.58; S, 11.55. ^{1}H NMR (400 MHz, Acetone) δ 7.60 (dd, J = 8.5, 1.5 Hz, 2H, H-3' & H-5'), 7.27 (dd, J = 7.9, 1.6 Hz, 2H, H-2' & H-6'), 6.93 (dddd, J = 18.6, 8.2, 6.7, 1.4 Hz, 2H), 6.75 (t, J = 7.8 Hz, 1H), 6.62 (d, J = 8.1 Hz, 1H), 6.22 (dd, J = 7.4, 1.1 Hz, 1H), 5.24 (s, 2H), 2.89 (s, 14H), 2.06 (p, J = 1.8 Hz, 4H). The spectra of TCM are given in appendix D.

3.3.2.3.   N-(2,4-dichlorophenyl)-N-(2-(4-(piperidin-1-ylsulfonyl)benzylamino)ethyl)methane sulfonamide (DCP)

The fragment DCP with the formula C21H27Cl2N3O4S2 is given above. It is solid, white in color, having a molecular weight of 520.49 g/mol, a melting point of 125 ℃, and is soluble in DMSO and chloroform. IR (cm^{-1}) V$_{max}$: 3277 (N-H), 2825 (Ar-H), 1334 (SO$_2$ stretching), 1166 (C-N stretching), 1091 (C-O stretching); HRMS (*m/z*): [M+1] 520.08 (13%), 519.08 (24%), 281.98 (68%), 238.09 (75%), 147.97 (64%), 91.05 (100.0%). Anal. Calcd: C, 48.46; H, 5.23; N, 8.07; S, 12.32. Found: C, 48.50; H, 5.28; N, 8.12; S, 12.37. ^{1}H NMR (400 MHz, Acetone) δ 7.75–7.33 (m, 4H, H-3', H-5', H-3'' and H-6''), 7.17 (dd, J = 8.6, 2.4 Hz, 2H, H-2', H-6'), 6.98 (d, J = 8.6 Hz, 1H, H-5''), 3.46 (s, 1H, H-7''), 2.72 (dt, J = 18.6, 6.8, 2.8 Hz, 4H, H-2 and H-6), 2.10–1.65 (m, 2H, H-4), 1.43 (p, J = 5.7 Hz, 2H, H-3 and H-5), 1.29 (d, J = 5.5 Hz, 2H, CH2-9'), 1.16 (s, CH$_3$, 3H), 1.06 (d, J = 6.6 Hz, 2H, CH2-8'). The spectra of DCP are given in appendix D.

3.3.2.4.   N-(2-(4-(piperidin-1-ylsulfonyl)benzylamino)ethyl)-N-(2,4,5-trichloro-phenyl)methane sulfonamide (TCP)

The fragment TCP with the formula C21H26Cl3N3O4S2 is given above. It is solid, light brown in color, having a molecular weight of 554.94 g/mol, a melting point of 153 ℃, and is soluble in DMSO and chloroform. IR (cm^{-1}) V$_{max}$: 3189 (N-H), 2814 (Ar-H), 1325 (SO$_2$ stretching), 1158 (C-N stretching), 1099 (C-O stretching); HRMS (*m/z*): [M$^+$] 553.04 (15.0%), 315.59 (98%), 319.94 (3.5%), 238.32 (73%), 147.97 (64%), 91.05 (100.0%). Anal. Calcd: C, 45.45; H, 4.72; N, 7.57; S, 11.56. Found: C, 45.50; H, 4.77; N, 7.62; S, 11.61. ^{1}H NMR (400 MHz, DMSO) δ 7.71 (dd, J = 8.3, 6.6 Hz, 2H, H-3' and H-5'), 7.62–7.52 (m, 2H, H-3'' and H-6''), 6.74–6.66 (m, 2H, H-2' and H-6'), 4.55 (d, J = 6.0 Hz, 2H, CH2-9'), 4.03 (brs, 2H, CH2-7'), 3.62 (t, J = 4.7 Hz, 4H, H-2 and H-6), 3.16–3.10 (m, 2H, H-8'), 2.86 (q, J = 6.0 Hz, 4H, H-3 and H-5), 2.09 (s, 3H, CH$_3$), 1.51-1.24 (m, 2H, H-4). The spectra of TCP are given in appendix D.

3.3.3. Biological Assay Results

To provide the safety profile of these four promising compounds, firstly they have been tested on HGFs, at 10 and 50 μM for 48 h, comparing the results with the vehicle DMSO, assumed as control. The results reported in Figure 28 demonstrated that at 10 μM, the four compounds didn't affect the cell viability of healthy cells, disregarding the substitution pattern, with respect to DMSO (**Figure 8A**).

At 50 μM (**Figure 8B**), TCP and DCP show the same result, whereas a statistically significant reduction in cell viability is evidenced when TCM and DCM are administered with respect to DMSO, with a major extent for DCM (52% of cell viability), even if the cell viability rate never goes under 50%. Thus, for the four compounds we can assume an IC50 > 50 μM at 48 h.

After 72 h of treatment, when the newly synthesized compounds are administered at 10 μM, a lower viability level is recorded in the presence of TCM (89.9% of cell viability), while, TCP, DCP and DCM do not show any significant modification of HGF viability with respect to control sample (DMSO) (**Figure 8C**). At 50 μM the previous trend recorded

508
509
510
511
512
513
514
515
516
517
518
519
520
521
522
523
524
525
526
527
528
529
530
531
532
533
534
535
536
537
538
539
540
541
542
543
544
545
546
547
548
549
550
551

after 48 h was confirmed (IC$_{50}$ >50 μM), recording a slight but statistically significant alteration of the non-cancerous cells viability (IC$_{50}$ ranging between 10 and 50 μM) after DCP and DCM administration (**Figure 8D**).
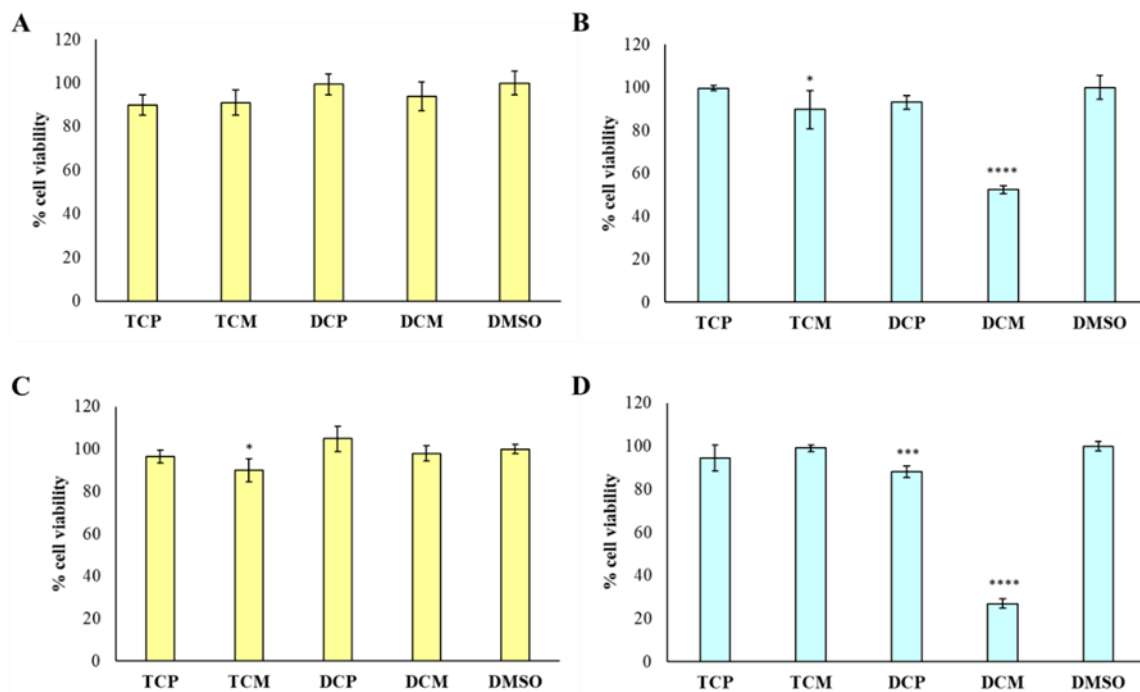

Figure 8. MTT test on HGFs treated with the hit compounds.

MTT test on HGFs treated with TCP, TCM, DCP and DCM compounds at 10 μM (left histograms) and 50 μM (right histograms) for 48 h (A and B) and 72 h (C and D); DMSO: control vehicle. Data are presented as mean % ± SD. The most representative of three different experiment is shown.

B * vs DMSO p=0.0357. **** vs DMSO p < 0.0001; C * vs DMSO p=0.0149; D *** vs DMSO p=0.0002, **** vs DMSO p < 0.0001.

Then, the capability of the novel compounds to affect the viability of gastric adenocarcinoma AGS cell line at 50 μM (maximum concentration in the previous experiment) after 48 (**Figure 9A**) and 72 h (**Figure 9B**) of treatment, has been determined.

After 48 h of treatment, the cell viability percentage appears significantly reduced in the presence of TCP, DCP and DCM compared to DMSO, with a major extent for DCM which leads to record an extremely low cell viability rate (5.7%). After 72 h of treatment, DCP still discloses a significant reduction of cell viability even if it is estimated to be of 96%, approximately. Conversely, DCM does not allow a AGS recovering considering that, after 72 h of treatment, the effect appears to be still strong keeping the cell viability level at very low percentages (6.8%). Thus, it can be argued that TCP, TCM and DCP are well tolerated to AGS even if a slight lower cell viability percentage with respect to HGFs (IC$_{50}$ >50 μM) can be highlighted. On the contrary, DCM exerts a marked and pronounced effect on tumoral cell viability with respect to healthy HGFs (IC$_{50}$ <50 μM). These results pinpoint how slight differences in the substitution pattern (the chlorine atom at position 5 in the morpholino series) could influence the selection of the administration dose to avoid unpleasant side effects.
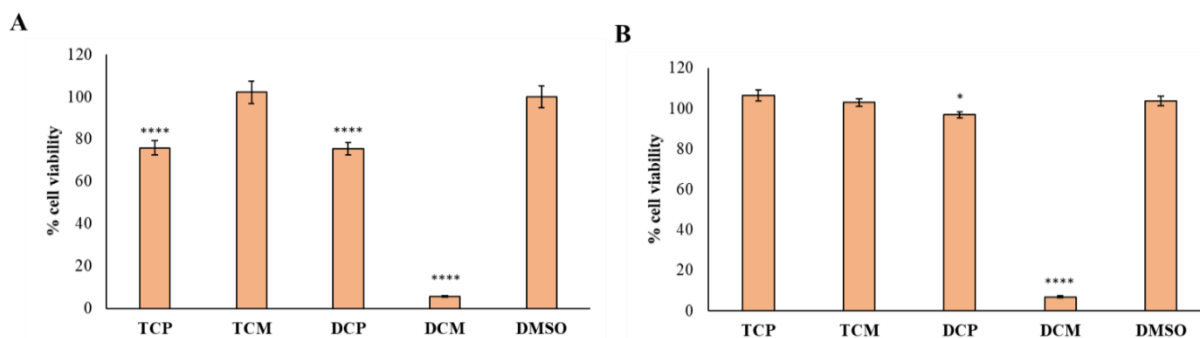
574

Figure 9. MTT test on AGS treated with the hit compounds.

MTT test on AGS treated with TCP, TCM, DCP and DCM at 50 µM for 48 h (A) and 72 h (B); DMSO: control vehicle. Data are presented as mean % ± SD. The most representative of three different experiment is shown. A **** vs DMSO p < 0.0001; B * vs DMSO p=0.0172, **** vs DMSO p < 0.0001.

575

3.3.4. Surface Plasmon Resonance (SPR)

Determination of dissociation equilibrium constant (KD) by SPR

SPR technique is efficient biophysical method for determination of affinity and kinetics of synthesized compounds with target proteins. The terms in SPR are little different from conventional terminology. The ligand referred to the interactant attached on sensor surface while analyte referred as the interactant present in sample solution injected over the surface. There are number of coupling methods available for SPR studies depending on target analyte and ligand.

In the presented study, we firstly tried the amine coupling method adopted from the Hyun Lee work [54]. The amine coupling method did not worked for our Hepatitis C Virus (HCV-1a) NS3 protease/helicase immunodominant region Protein (aa 1356-1459, GST tag). As the used ligand was not stable enough for supporting amine coupling. After amine coupling, we tried the GST coupling method for SPR study of our one of the hits TCM. It is important to find out suitable immobilization pH prior immobilization. For the two different PH buffers (Sodium acetate buffer pH -5.0 and pH 4.5) were used. The response (RU) was dropped at lower pH so the immobilization buffer of pH 5.0 was proceeded for immobilization (Sensorgram 1). The sensorgram begins flattening out after the covalent coupling, which may contribute to the robustness of assay. The graphs of pH scouting are given in appendix E.
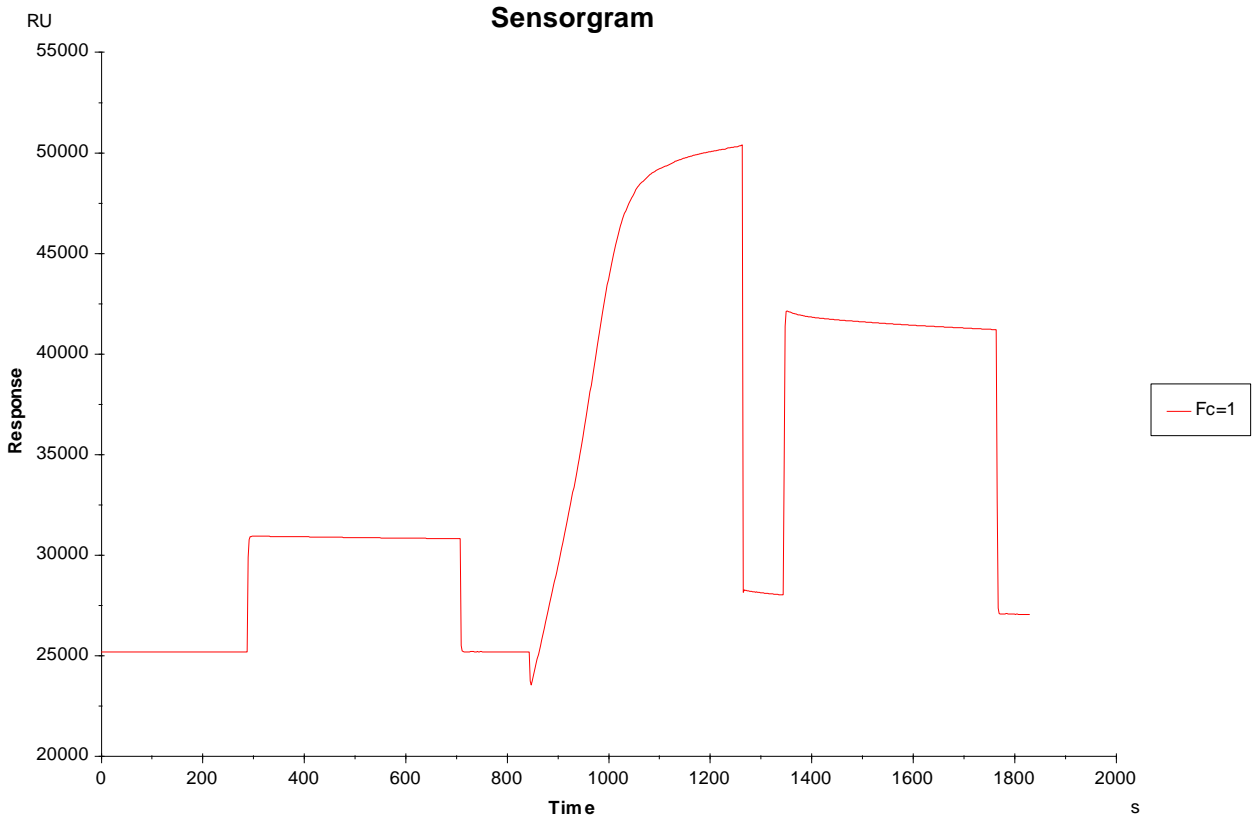
576
577
578
579
580
581
582
583
584
585
586
587
588
589
590
591
592
593
594
595

Figure 10. Sensogram graph.

following parameters were set for Immobilization wizard:
Immobilization Setup
————————

```
Chip type                  CM5
Flow cells per cycle       2


Flow cell 1,2
————————

Specify contact time and flow rate
Method                     S200 Amine
Ligand                     antiGST 30 ug/mL
Contact Time               420 (s)
Flow rate                  10 (µl/min)
```

The theoretical Rmax value calculated is 54.78 from1864.2 RU, MWA 556.91 Da, MWL 37900 Da and SM 2. The Rmax value was calculated by using following equation:

$$R_{max} = \frac{MWA}{MWL} * SM * RU$$

Where,
Rmax= Theoretical maximum binding Capacity
MWA= Molecular weight Analyte (Da)
MWL= Molecular weight Ligand (Da)
SM= Stoichiometric Ratio (theoretical value of binding of analyte molecule to ligand, here is 1:2)
RU= Immobilized amount

Single cycle runs were used for small molecule binding analysis. The buffer used to prepare the protein samples was HBS-EP (20 mM HEPES, 150 mM NaCl, 10 mM MgCl$_2$, 0.01% Tween 20, pH = 7.4). For runs with small molecules, an additional 1% DMSO was added for solubility. GST capture kit conditions (Cytiva catalog number BR100223) were used to capture anti-GST antibody on both the sample and reference cells (7 min immobilization, 10 µL/min flow rate). Both surfaces had high affinity sites capped with an additional 3 min of GST flowed over (5 µg/mL concentration, 5 µL/min flow rate) followed by regeneration (10 mM glycine, pH = 2.2). On the subtractive reference surface, GST was immobilized (10 µg/mL, 5 µL/min, 5 min). On the sample surface, GST-tagged HCV was immobilized in a similar fashion (10 µg/mL, 5 µL/min, 5 min). The wizard parameters for single cell kinetics are given in appendix F.

The experimental Rmax of TCM as function time was found 8.1 in FC 2-1 and KD value 1.01X10-11.   The five concentrations 2.4, 12, 60, 300, 1500 uM were formed for TCM to study dose-response curve as shown (Fig. 1C), the following curve show the increase in response with sample concentration till 50 nM with RU 39.4 and keep increasing on higher concentration. These results gave encouragement to explore the other hits for the SPR binding and kinetics study. The dose response should be optimized further for more data points.

The experimental Rmax of TCM as function time was found 8.1 in FC 2-1 and KD value 1.01X10-11. The five concentrations 2.4, 12, 60, 300, 1500 uM were formed for TCM to study dose-response curve as shown (Fig. 1C), the following curve show the increase in response with sample concentration till 50 nM with RU 39.4 and keep increasing on higher concentration. These results gave encouragement to explore the other hits for the

SPR binding and kinetics study. The dose response should be optimized further for more data points.
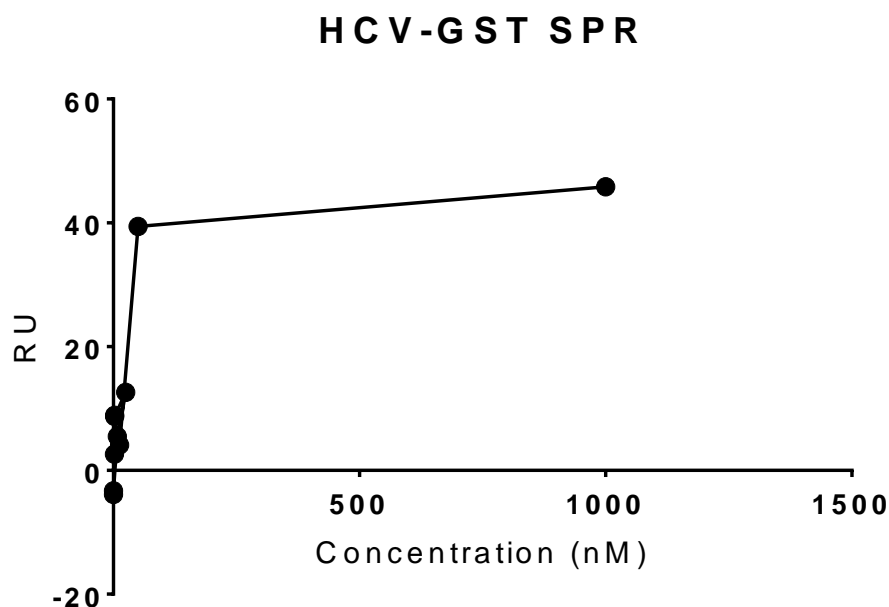
HCV-GST SPR

Figure 11. Response versus concentration graph.

5. Conclusions

The computational chemistry, medicinal chemistry, and bioinformatics approaches have been employed to find protease inhibitors. This interdisciplinary methodology has enabled to analyze the problem under wider scope. The study has revealed that theoretical results are corroborated by experimental findings. The molecular dynamics and pharmacokinetics studies revealed that the hit compounds ZINC000224449889, ZINC000224374291, and ZINC000224374456 and derivative of ZINC000224374456 are potential drug contenders against HCV NS3 protease genotype 3a. The optimized compounds namely TCP, TCM and DCP displayed a safe profile of cell viability (HGFs versus AGS) up to 50 μM, whereas DCM should be administered at lower concentrations.

We got the limited time facility for SPR and TCM was selected for SPR studies to evaluate the binding and kinetics of the compounds against GST-HCV NS/34A protein. The group was able to purchase NS3/4A 1b GST tag HCV protein while NS3/4A 3b genotype is not available as isolated recombinant protein for assay. SPR assay was developed for HCV by hit and trial method. It was found that GST capture approach is effective for the HCV SPR assay. There is need for the availability of our target genotype recombinant polyprotein for further exploration of hits for target specific studies. Preliminary SPR results demonstrated that TCM was bound in 1:1 binding mode with target protein and was found effective at 50 nM concentration. We have aim to run SPR assays of other hits on availability of SPR facility in future.

Author Contributions: Rashid: Conceptualization; methodology; formal analysis; investigation; data curation; writing—original draft preparation; computational studies, preliminary synthesis. Zulkarnain: writing, synthesis, characterization, investigation. Hira and Simone: writing—review and editing; project design and management, characterization; supervision, investigation; SPR studies. Qaiser: review and editing; supervision. Susi and Amelia: cell-based assays.

Appendix A

Hardware and software.

Appendix B

Synthesis of fragments the hit compounds.

Appendix C

Spectra of fragments the hit compounds.

Appendix D

Spectra of the hit compounds.

Appendix E

SPR pH scouting.

Appendix F

SPR wizard parameters for single cell kinetics.

References

1. Choo, Q. L.; Kuo, G.; Weiner, a J.; Overby, L. R.; Bradley, D. W.; Houghton, M. Isolation of a CDNA Clone Derived from a Blood-Borne Non-A, Non-B Viral Hepatitis Genome. *Science* **1989**, *244* (4902), 359–362. https://doi.org/10.1126/science.2523562.

2. Hanafiah, K. M.; Groeger, J.; Flaxman, A. D.; Wiersma, S. T. Global Epidemiology of Hepatitis C Virus Infection: New Estimates of Age-Specific Antibody to HCV Seroprevalence. *Hepatology* **2013**, *57* (4), 1333–1342.

3. Ferri, C.; Sebastiani, M.; Giuggioli, D.; Colaci, M.; Fallahi, P.; Piluso, A.; Antonelli, A.; Zignego, A. L. Hepatitis C Virus Syndrome: A Constellation of Organ- and Non-Organ Specific Autoimmune Disorders, B-Cell Non- Hodgkin's Lymphoma, and Cancer. *World J. Hepatol.* **2015**, *7* (3), 327–343. https://doi.org/10.4254/wjh.v7.i3.327.

4. Rusyn, I.; Lemon, S. M. Mechanisms of HCV-Induced Liver Cancer: What Did We Learn from in Vitro and Animal Studies? *Cancer Lett.* **2014**, *345* (2), 210–215. https://doi.org/10.1016/j.canlet.2013.06.028.

5. Borgia, S. M.; Hedskog, C.; Parhy, B.; Hyland, R. H.; Stamm, L. M.; Brainard, D. M.; Subramanian, M. G.; McHutchison, J. G.; Mo, H.; Svarovskaia, E.; Shafran, S. D. Identification of a Novel Hepatitis C Virus Genotype From Punjab, India: Expanding Classification of Hepatitis C Virus Into 8 Genotypes. *J. Infect. Dis.* **2018**, *218* (11), 1722–1729. https://doi.org/10.1093/infdis/jiy401.

6. Smith, D. B.; Bukh, J.; Kuiken, C.; Muerhoff, A. S.; Rice, C. M.; Stapleton, J. T.; Simmonds, P. International Committee on Taxonomy of Viruses (ICTV). HCV Classification. A Web Resource to Manage the Classification and Genotype and Subtype

Assignments of Hepatitis C Virus. *(https://talk.ictvonline.org/ictv_wikis/flaviviridae/ w/sg_flavi/56/hcv-classification)* **2017**.   720

7.   Hara, K.; Rivera, M. M.; Koh, C.; Sakiani, S.; Hoofnagle, J. H.; Heller, T. Important Factors in Reliable Determination of   721
Hepatitis C Virus Genotype Using the 5' Untranslated Region. *J. Clin. Microbiol.* **2013**, JCM--03344.   722

8.   Gentzsch, J.; Brohm, C.; Steinmann, E.; Friesland, M.; Menzel, N.; Vieyres, G.; Perin, P. M.; Frentzen, A.; Kaderali, L.;   723
Pietschmann, T. Hepatitis C Virus P7 Is Critical for Capsid Assembly and Envelopment. *PLoS Pathog.* **2013**, *9* (5), e1003355.   724

9.   Bartenschlager, R.; Cosset, F.-L.; Lohmann, V. Hepatitis C Virus Replication Cycle. *J. Hepatol.* **2010**, *53* (3), 583–585.   725

10.   Pike, R. Special Article The Molecular Virology of Hepatitis C. *Hepatology* **1989**.   726

11.   Taylor, C. M.; Wang, Q.; Rosa, B. A.; Huang, S. C.-C.; Powell, K.; Schedl, T.; Pearce, E. J.; Abubucker, S.; Mitreva, M. Discovery   727
of Anthelmintic Drug Targets and Drugs Using Chokepoints in Nematode Metabolic Pathways. *PLoS Pathog.* **2013**, *9* (8),   728
e1003505.   729

12.   Chae, T. U.; Choi, S. Y.; Kim, J. W.; Ko, Y.-S.; Lee, S. Y. Recent Advances in Systems Metabolic Engineering Tools and   730
Strategies. *Curr. Opin. Biotechnol.* **2017**, *47*, 67–82.   731

13.   Riaz, M. R.; Preston, G. M.; Mithani, A. MAPPS: A Web-Based Tool for Metabolic Pathway Prediction and Network Analysis   732
in the Postgenomic Era. *ACS Synth. Biol.* **2020**, *9* (5), 1069–1082.   733

14.   Grakoui, A.; McCourt, D. W.; Wychowski, C.; Feinstone, S. M.; Rice, C. M. Characterization of the Hepatitis C Virus-Encoded   734
Serine Proteinase: Determination of Proteinase-Dependent Polyprotein Cleavage Sites. *J. Virol.* **1993**, *67* (5), 2832–2843.   735

15.   Gorbalenya, A. E.; Donchenko, A. P.; Koonin, E. V; Blinov, V. M. N-Terminal Domains of Putative Helicases of Flavi- and   736
Pestiviruses May Be Serine Proteases. *Nucleic Acids Res.* **1989**, *17* (10), 3889–3897.   737

16.   Failla, C.; Tomei, L.; De Francesco, R. Both NS3 and NS4A Are Required for Proteolytic Processing of Hepatitis C Virus   738
Nonstructural Proteins. *J. Virol.* **1994**, *68* (6), 3753–3760.   739

17.   Ashraf, M. U.; Iman, K.; Khalid, M. F.; Salman, H. M.; Shafi, T.; Rafi, M.; Javaid, N.; Hussain, R.; Ahmad, F.; Shahzad-Ul-   740
Hussan, S.; Mirza, S.; Shafiq, M.; Afzal, S.; Hamera, S.; Anwar, S.; Qazi, R.; Idrees, M.; Qureshi, S. A.; Chaudhary, S. U.   741
Evolution of Efficacious Pangenotypic Hepatitis C Virus Therapies. *Med. Res. Rev.* **2019**, *39* (3), 1091–1136.   742
https://doi.org/10.1002/med.21554.   743

18.   Hussain, R.; Khalid, H.; Fatmi, M. Q. Molecular Modeling Approach of Serine Protease NS3-4A Genotype 3a as a Potential   744
Drug Target of Hepatitis C Virus: Homology Modeling and Virtual Screening Study. *J. Comput. Biophys. Chem.* **2021**, *20* (06),   745
631–639.   746

19.   Hussain, R.; Khalid, H.; Fatmi, M. Q. HCV Genotype-Specific Drug Discovery through Structure-Based Virtual Screening.   747
Pure Appl. Chem. **2022**, 1–10. https://doi.org/10.1515/pac-2021-1104.   748

20.   Alagöz, M. A.; Özdemir, Z.; Uysal, M.; Carradori, S.; Gallorini, M.; Ricci, A.; Zara, S.; Mathew, B. Synthesis, Cytotoxicity and   749
Anti-Proliferative Activity against AGS Cells of New 3 (2 H)-Pyridazinone Derivatives Endowed with a Piperazinyl Linker.   750
Pharmaceuticals **2021**, *14* (3), 183.   751

21.   Li, K.-B. ClustalW-MPI: ClustalW Analysis Using Distributed and Parallel Computing. *Bioinformatics* **2003**, *19* (12), 1585–1586.   752

22.   Ramachandran, G. N.; Ramakrishnan, C.; Sasisekharan, V. Stereochemistry of Polypeptide Chain Configurations. *J. Mol. Biol.*   753
1963, *7* (1), 95–99. https://doi.org/10.1016/S0022-2836(63)80023-6.   754

23.   Sterling, T.; Irwin, J. J. ZINC 15 - Ligand Discovery for Everyone. *J. Chem. Inf. Model.* **2015**, *55* (11), 2324–2337.   755
https://doi.org/10.1021/acs.jcim.5b00559.   756

24.   Allen, W. J.; Balius, T. E.; Mukherjee, S.; Brozell, S. R.; Moustakas, D. T.; Lang, P. T.; Case, D. A.; Kuntz, I. D.; Rizzo, R. C.   757
DOCK 6: Impact of New Features and Current Docking Performance. *J. Comput. Chem.* **2015**, *36* (15), 1132–1156.   758

25.   Van Der Spoel, D.; Lindahl, E.; Hess, B.; Groenhof, G.; Mark, A. E.; Berendsen, H. J. C. GROMACS: Fast, Flexible, and Free.   759
J. Comput. Chem. **2005**, *26* (16), 1701–1718.   760

26.   Kulig, W.; Pasenkiewicz-Gierula, M.; Róg, T. Topologies, Structures and Parameter Files for Lipid Simulations in GROMACS   761

with the OPLS-Aa Force Field: DPPC, POPC, DOPC, PEPC, and Cholesterol. *Data Br.* **2015**, *5*, 333–336.

27. Jiang, F.; Zhou, C.-Y.; Wu, Y.-D. Residue-Specific Force Field Based on the Protein Coil Library. RSFF1: Modification of OPLS-AA/L. *J. Phys. Chem. B* **2014**, *118* (25), 6983–6998.